A Storyline Approach to the June 2021 Northwestern North American Heatwave

Laurent Terray[1]

[1]CERFACS

November 26, 2022

Abstract

Northwestern North America has experienced an exceptional heatwave in late June 2021 with many new temperature records across western Canada, Oregon and Washington states. Here we use a recent atmospheric reanalysis and a conditional approach based on dynamical adjustment to assess and quantify the influence of atmospheric circulation and other driving factors to the heatwave magnitude during the June 28–30 period. A blocking anticyclone, enhanced low-level moisture and clear-sky downward long-wave radiation are shown to be the main factors of the heatwave persistence and magnitude. The heatwave magnitude is mainly attributable to internal variability with climate change being an additional factor (10%). Consequences of a similar atmospheric circulation anomaly in different phases of the Atlantic Multidecadal and Pacific Decadal Oscillations and in a warmer world at different global warming levels (1, 2, 3 and 4°C) are explored based on a single model initial-condition large ensemble.

Hosted file

`essoar.10512596.1.docx` available at https://authorea.com/users/530449/articles/606005-a-storyline-approach-to-the-june-2021-northwestern-north-american-heatwave

Hosted file

`grl_suppinfo.docx` available at https://authorea.com/users/530449/articles/606005-a-storyline-approach-to-the-june-2021-northwestern-north-american-heatwave

Laurent Terray[1]

[1]CECI, Université de Toulouse, CERFACS/CNRS, Toulouse, France.

Corresponding author: Laurent Terray (terray@cerfacs.fr)

Key Points:

- A blocking ridge, enhanced moisture and clear-sky downward long-wave radiation are the main causes of the heatwave magnitude and duration.
- The phase of the Pacific decadal oscillation can influence the pattern and magnitude of the circulation-induced heatwave component.
- A similar blocking event in a 2°C warmer climate would lead to a 4°C increase of the circulation-induced heatwave component.

Abstract

Northwestern North America has experienced an exceptional heatwave in late June 2021 with many new temperature records across western Canada, Oregon and Washington states. Here we use a recent atmospheric reanalysis and a conditional approach based on dynamical adjustment to assess and quantify the influence of atmospheric circulation and other driving factors to the heatwave magnitude during the June 28–30 period. A blocking anticyclone, enhanced low-level moisture and clear-sky downward long-wave radiation are shown to be the main factors of the heatwave persistence and magnitude. The heatwave magnitude is mainly attributable to internal variability with climate change being an additional factor (10%). Consequences of a similar atmospheric circulation anomaly in different phases of the Atlantic Multidecadal and Pacific Decadal Oscillations and in a warmer world at different global warming levels (1, 2, 3 and 4°C) are explored based on a single model initial-condition large ensemble.

Plain Language Summary

Gathering robust statistics and performing extreme event attribution for very rare heat extreme events, such as the 2021 Northwestern North American heatwave, remain challenging due to incomplete sampling of weather data (~100 years) challenging the application of extreme value theory and caveats related to the use of imperfect climate models in estimating likelihood changes between worlds with and without human influence. Here we use the dynamical adjustment method to quantify the key factors responsible for the magnitude and persistence of the heatwave. Dynamical adjustment aims to identify the causal factors that led to the heatwave with an approach conditional on the observed atmospheric circulation during the event. We find that natural variability is the main driver of the heatwave extreme magnitude with a small contribution from climate change. While the main contribution comes from the atmospheric circulation-related component (the dynamic component), we also suggest a small contribution due the negative phase of the Pacific Decadal Oscillation observed in June 2021. Finally, we ask whether future climate change can make a future

similar event even more extreme. We find that the dynamic component would increase by 4°C in a 2°C warmer global climate.

1 Introduction

An exceptional heatwave occurred during late June – early July 2021 across western Canada and several U.S. States, Oregon and Washington in particular (Overland 2021). During the 28–30 June period, many maximum temperature records were broken in Canada and U.S. Pacific Northwest, including the Canada all-time daily maximum temperature record with 49.6°C in Lytton on June 29th. The likelihood of this unprecedented event is very difficult to assess statistically due to its exceptional magnitude compared to the historical record. A recent extreme attribution study finds that the event is estimated to be about a 1 in 1000-yr event in current climate and would have been 150 times rarer in a pre-industrial unperturbed climate (Philip et al., 2021).

The chain of atmospheric dynamical processes preceeding and leading to the heatwave has been analyzed in Neal et al. (2022). Based on a local wave activity diagnostic, they show the importance of a diabatic heating source associated with a storm off the Alaskan coast a few days earlier in driving the blocking anticyclone that ultimately led to the heatwave. Sub-seasonal to seasonal climate prediction systems were able to predict the occurrence of an anomalous warming as early as June 10th 2021 (three weeks in advance) but no forecasts issued before June 17th was able to predict the correct magnitude of the event (Lin et al., 2022). The latter paper has suggested that two important dynamical processes contributed to the heatwave magnitude: an upper tropospheric wave train associated with the boreal summer intraseasonal oscillation in Southeast Asia and an anomalous North Pacific atmospheric river leading to high moisture conditions over the heatwave region.

Building on the above studies, here we investigate and quantify the different contributions to this extreme event by using the dynamical adjustment methodology and a state-of-the-art reanalysis. We also perform a simple analysis of the surface heat budget to assess the key physical processes responsible for the extreme magnitude of the event. Based on a climate model historical and pre-industrial simulations, we then investigate and quantify the potential influence of low-frequency internal climate variability modes such as the Pacific Decadal Oscillation (PDO) and the Atlantic Multidecadal Oscillation (AMO) on the contribution of the atmospheric circulation-related component to the heatwave pattern and magnitude. Finally, we use multi-member climate projections from a climate model to look at the consequences of an atmospheric circulation similar to that observed in late June 2021 but occurring in warmer climates with increasing global warming level.

2 Data and Methods

2.1 Atmospheric reanalysis and observed datasets

We use the ERA5 reanalysis as our main dataset (Hersbach et al., 2020, Bell

et al., 2021). The circulation variable is the daily 500-hPa geopotential height (Z500) and the characterization of the heatwave is based on the daily maximum 2–meter temperature (TX). We also make use of surface temperature and heat fluxes, both radiative and turbulent. We use the full 1950-2021 period for the dynamical adjustment of ERA5 obtained by merging the recent 1979–2021 period with the 1950–1978 one named as the "back extension". All results showing TX or Z500 anomalies are based on the 1991–2020 climatological period.

2.2 Model data

We use Z500 and TX daily data from the CESM2 large ensemble (Rodgers et al., 2021). We use 20 members, originally numbered 1–10 and 91–100 of the historical and ssp370 scenario simulations. The different members differ by their initial conditions that are 10 years apart within the ending period (1000–1200yr) of the CESM2 pre-industrial control simulation (picntrl). The CESM2 picntrl daily data is also used to assess the PDO and AMO influence. To ease the comparison between CESM2 and ERA5 dynamical adjustment results, the ERA5 data is interpolated onto the CESM2 grid.

2.3 Methods

2.3.1 Definition of the heatwave period and region

To define the heatwave period (June 28–30, 2021), we select the most intense 3–day period in term of the daily maximum temperature for a region (the heatwave region thereafter, see Figure 1a) that encompasses the majority of stations with broken temperature records during the heatwave (45°–56°N; 123°–114°W). Note that our main findings are robust to small spatial and temporal variations of the region and heatwave period. We also use an extended region (a large western Canada box) for some analyses.

2.3.2 Dynamical adjustment with observations

Within the framework of extreme event attribution, dynamical adjustment can be defined as a singular/conditional approach that takes the atmospheric circulation during the event as given and then tries to identify the key causal factors that led to the extreme event (Lloyd and Shepherd, 2020). Here we use the approach described in Terray (2021) to identify the main drivers of the 2021 northwestern North American heatwave. The approach is based on constructed analogues of the atmospheric circulation that occurred during the event. Given a daily TX anomaly, dynamical adjustment seeks to isolate TX atmospheric circulation-related changes (the TX dynamic component thereafter or $\mathrm{DYN_{CF}}$). The residual ($\mathrm{RES_{TOT}}$) can then be attributed to both internal changes in land or ocean surface conditions ($\mathrm{RES_{INT}}$) and response to external forcing ($\mathrm{RES_{TRD}}$ and $\mathrm{RES_{FRC}}$). We refer to Terray (2021) and Text S1 in Supporting Information S1 for a more detailed description.

2.3.3 Dynamical adjustment with model data

Assuming that the observed anomalous atmospheric circulation can happen in

the model world, the CESM2 model framework can be used to assess the uncertainty of dynamical adjustment results associated with the limited length of the observed record (~72 years). The initial step is to interpolate ERA5 Z500 and TX daily anomalies (relative to the 1991–2020 period) onto the CESM2 model grid for all days of the extended heatwave period. For all CESM2 historical members, we then reconstruct the full Z500 model field during the heatwave period by adding these anomalies to the CESM2 model daily climatology calculated over the 1991–2020 period. Finally, we come up virtually with 20 different model realizations that experience the same anomalous atmospheric circulation at the same time as in the observations. We then apply the same dynamical adjustment approach as in the observations to all 20 members of the CESM2 model. We use the same period (1950–2021) as the observations in the model dynamical adjustment procedure. Assuming that the model provides a good analogue of the observed atmosphere-ocean system, a model-based uncertainty of the dynamic component estimation can then be assessed by estimating variations of the dynamic component among the 20 CESM2 members.

2.3.4 Trend estimation for atmospheric data

We use a Loess filter with a smoother length of 45 years, and we apply a light (3 years) additional smoothing of the trend before estimating the residual. When needed, we detrend the daily TX dataset separately for each month before applying the dynamical adjustment procedure. We assume that the TX trends derived from the Loess filter procedure are a reasonable estimate of the response to anthropogenic forcing (the forced component thereafter). The TX trend spatial patterns are shown in Figure S1 in Supporting Information S1.

2.3.5 Surface heat budget equation

The daily mean of the land surface heat budget equation can be written as:

$$Q = (1-\alpha)S^{\downarrow} + F^{\downarrow} + F^{\uparrow} - H - LE \quad (2)$$

where Q is the heat storage, the surface albedo, $S^{\downarrow}$ the surface downward shortwave radiation, $F^{\downarrow}$ and $F^{\uparrow}$ the surface downward and upward long-wave fluxes, H and LE the surface sensible and latent heat fluxes. $F^{\uparrow}$ can be approximated by $F^{\uparrow} \approx 4\sigma T_s^3$ with the emissivity (here taken as a constant) and T_s the surface temperature. Defining the reference as the 2021 June–July average and the perturbed state as the daily values, the perturbed surface heat equation (2) can be linearized and written as (Lu and Cai 2009):

$$4\sigma\overline{T_s}^3 T_s \approx -(\alpha)\left(\overline{S^{\downarrow}} + S^{\downarrow}\right) + CRF_s + (1-\overline{\alpha})\ S^{\downarrow,clr} + F^{\downarrow,clr} - Q - (H + LE) \quad (3)$$

where CRF_s is the surface cloud radiative forcing, indicates the perturbation given by the difference between the perturbed and reference states, the overbar denotes the reference mean state and $(.)^{clr}$ denotes clear-sky conditions for radiative fluxes. The RHS terms represent the surface albedo feedback (SAF), the change in surface cloud radiative forcing, the non-SAF-induced change in

clear-sky short-wave radiative flux, the change in downward clear-sky long-wave radiation flux, the change in heat storage, and the changes in surface sensible and latent fluxes, respectively. The contribution of each of these processes to the surface temperature change can be quantified as a partial temperature change obtained by dividing each of the RHS terms of equation (3) by $4\sigma\overline{T}_s^3$. The calculation is made at each ERA5 land grid-point with daily values for all physical variables.

3 Results

3.1 The June 2021 observed heatwave and key physical processes

We first show the extreme character of both heatwave magnitude and atmospheric circulation during the 2021 heatwave.

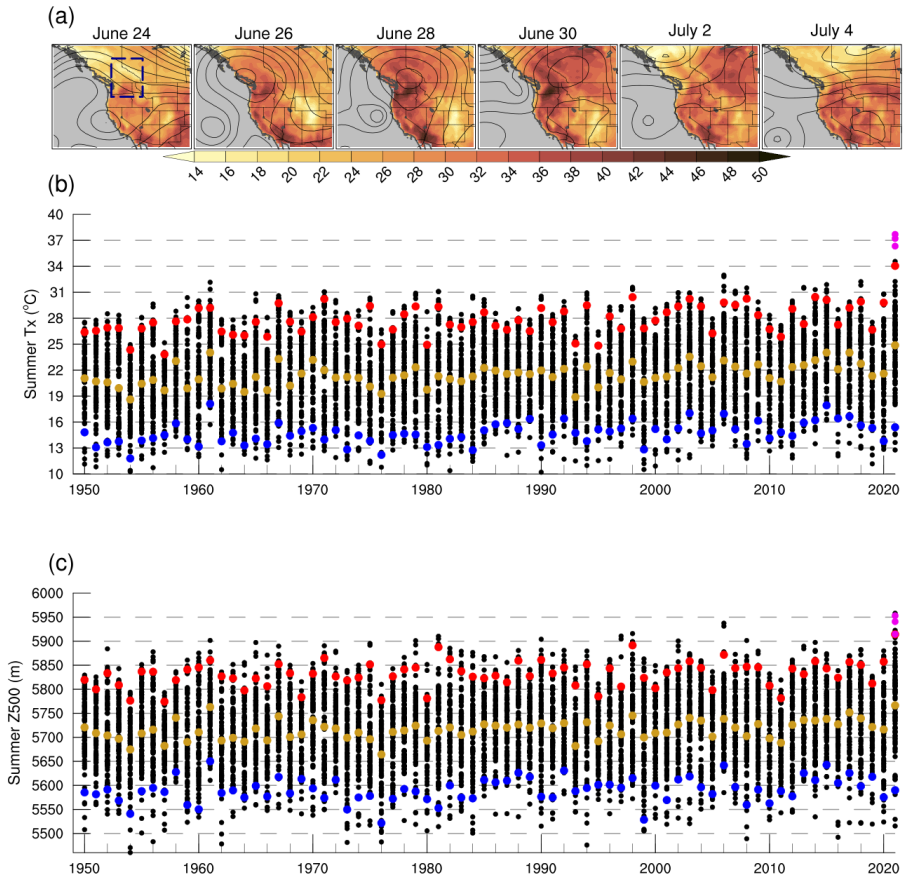

Figure 1. ERA5 daily maximum temperature (°C, shading) and geopotential height at 500hPa (m, contour) over northwestern North America: (a) Spatial patterns of the daily evolution of both TX and Z500 during the June 24 – July 4 period. The blue square indicates the heatwave region as defined in the main text. Z500 contours are spaced every 40 meters. (b) time evolution of daily summer (JJA) TX averaged over the heatwave region (black dots) for the 1950–2021 period. Blue, yellow and red dots represent the 5th, 50th (median) and 95th percentiles, respectively. Daily TX values during 28–30 June 2021 are shown with pink dots. (c) Same as (b) but for Z500.

Figure 1a shows that the Omega Block Z500 pattern (a sequence of low–high–low geopotential heights oriented eastward) is in formation over the Pacific ocean on

June 24. It then strengthens and slowly migrates eastward inland in conjunction with increasing TX over the Pacific Northwest land region. Extreme TX values (near 50°C) over the Pacific Northwest are reached during the June 28–30 period associated with the long-lasting and stationary blocking pattern. After July 1st, the blocking pattern decays and the mid-tropospheric circulation transitions to a more zonal flow pattern. Figure 1b shows the evolution of summer daily TX (area-averaged over the heatwave region, see region boundaries in Figure 1a) distribution since 1950. The three heatwave days (June 28–30) are unprecedented (breaking the previous record for the region-averaged TX by 4°C) and extraordinary events, all between 4- and 5-σ events relative to the June daily TX distribution. With regard to the region-averaged Z500, the June 28–30 days are also summer extremes (between 3- and 4-σ events with the maximum above 5950m) but not as much as TX: quasi-similar Z500 values also occurred in previous summers (years 2006, 1998, 1981 and 1961) that were also warm summers with high extreme (greater than the 95th percentile) TX values (Figures 1b and 1c). While a low-frequency increase in TX median can be visually depicted in Figure 1b, no such increasing trend is easily depicted for Z500 (Figure 1c).

Using equation (3) based on radiative and turbulent surface heat fluxes from ERA5, we now investigate the role of different processes that may have contributed to the extreme heatwave magnitude. Here we assume that surface temperature can be used to monitor the heatwave magnitude and persistence and identify the driving physical processes.

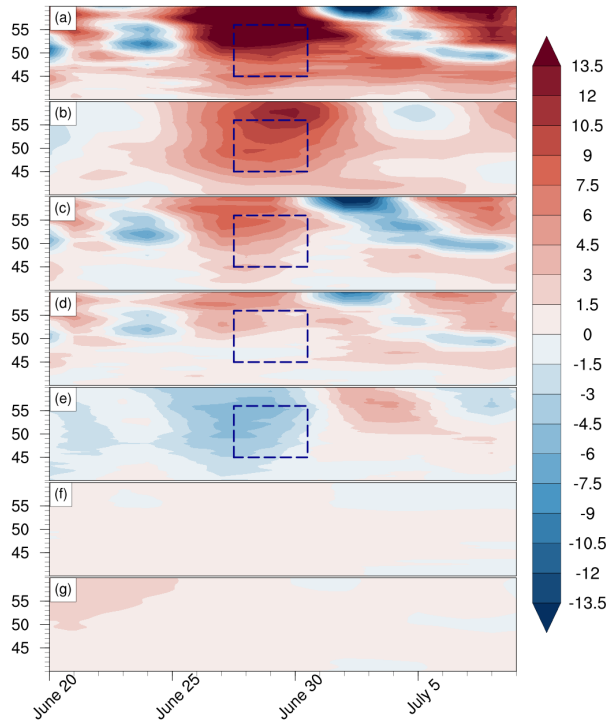

Figure 2. Latitude-time evolution of the ERA5 zonally-averaged surface temperature anomaly (K) over the region (40–60°N ;123–114°W): (a) the total temperature anomaly given by the sum of all partial contributions; the partial temperature changes due to (b) the change in net clear-sky long-wave radiation fluxes, (c) the change in surface cloud radiative forcing, (d) the changes in surface sensible/latent fluxes, (e) the change in heat storage, (f) surface albedo feedback (SAF), and (g) the non-SAF-induced change in clear-sky short-wave radiation, respectively. All physical terms have been smoothed with a 3-day running mean. The dashed line blue square indicates the latitudinal boundaries of the heatwave region and the heatwave period.

Figure 2 shows that the contribution of downward clear-sky long-wave flux to surface warming plays the dominant role in explaining the large magnitude of the heatwave as well as its persistence. The second contributor is cloud radiative forcing due to cloud-free skies and prolonged downward solar radiation (Figure 2c). The contributions of the turbulent (sensible and latent) heat fluxes and heat storage show smaller amplitude and partially cancel out over the heatwave region and period (Figures 2d and 2e). The other factors have a negligible

contribution to the heatwave magnitude and persistence. The key role of the downward clear-sky long-wave flux in the surface energy budget alludes to the importance of moisture and its transport from the Pacific ocean towards the continent in driving the magnitude and persistence of the heatwave as pointed out by Lin et al. (2022) (see their section 4.2). This is also corroborated by the large increase in moisture below 850 hPa over the heatwave region that originates from aloft on June 25th (see Text and Figure S2 in Supporting Information S1).

3.2 Dynamical component and its sensitivity to internal variability

We begin our attribution analysis with a complete decomposition of the 3-day heatwave TX anomaly (with 1991–2020 as baseline) into dynamic and residual components.

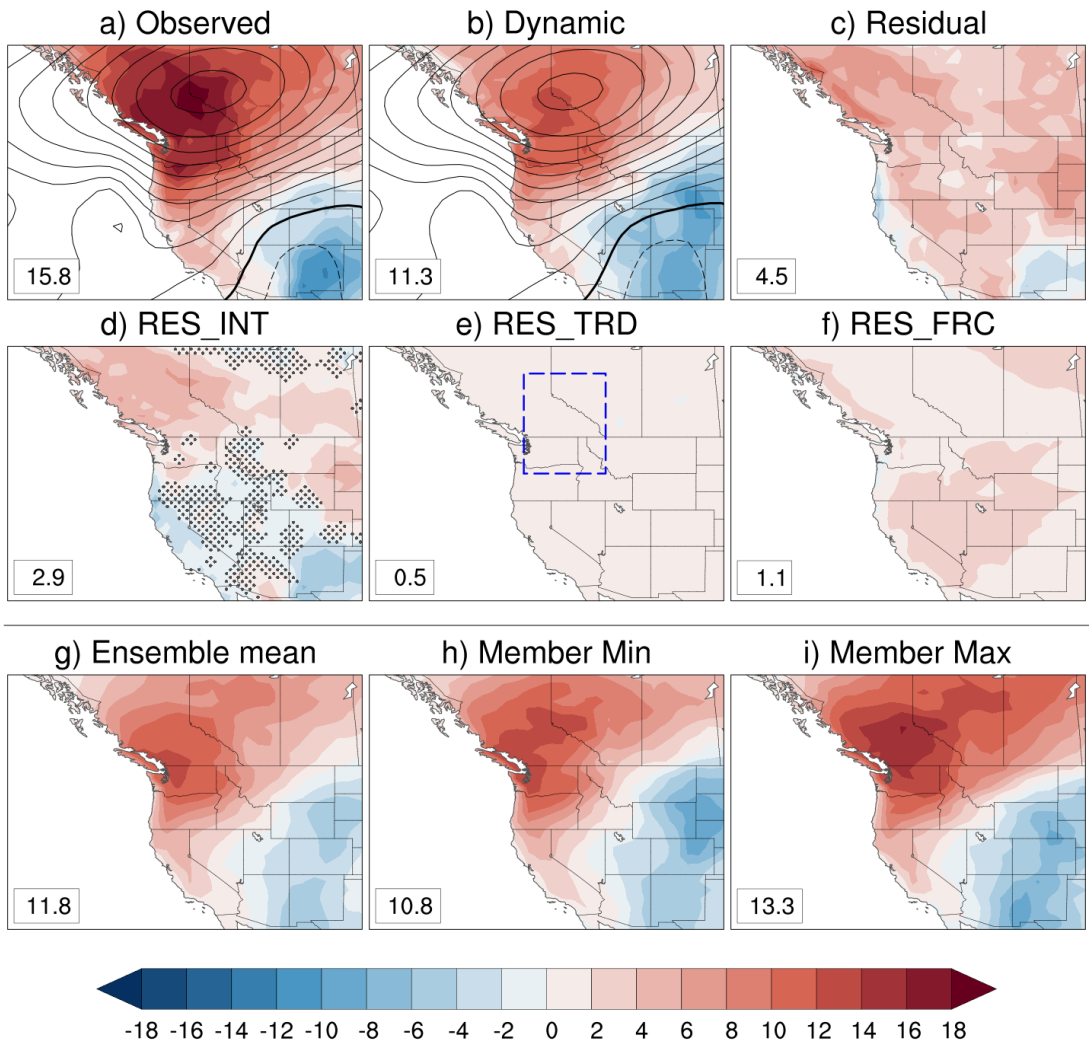

Figure 3. Decomposition of ERA5 daily TX anomaly (colors, °C) averaged over the June 28–30 period (°C) into dynamic and total residual contributions (a–c). In (a) and (b), contours indicate observed and reconstructed (by the dynamical adjustment method) Z500 anomalies, respectively. The contour interval is 25m, with dashed lines indicating negative values and the thick solid line the zero contour. Decomposition of the total residual in internal (RES_{INT}) and forced (RES_{TRD} and RES_{FRC}) components (d–f). CESM2 TX dynamic component: (g) 20-member ensemble mean, (h) member with smallest TX anomaly averaged over heatwave region, (i) member with largest TX anomaly averaged

over heatwave region. Numbers in lower-left corner indicate the TX anomaly spatial average over the heatwave region (dash line blue rectangle in (e)). In (d), stippling indicates grid points where RES_{INT} values are within the uncertainty range of the dynamical component given by the 95 % confidence interval estimated by the bootstrap method described in Terray (2021).

Figures 3a and 3b show that ~72% of the heatwave magnitude is due to to the dynamic component. The TX dynamic component exhibits a large-scale dipolar pattern with intense warm TX anomalies over the western U.S and northern Canada and cold TX anomalies in the southwest and central U.S (in agreement with southward advection of colder air masses from central Canada). The area with maximum TX anomaly is located under and southwest of the blocking ridge center, suggesting the possible contribution of other processes than adiabatic subsidence and solar heating (see above).

The total residual contribution (~4.5°C, Figure 3c) mainly comes from the TX internal residual component (~2.9°C) and to a lesser extent from the RES_{FRC} term (~1.1°C). Together, they represent ~25% of the heatwave magnitude over the heatwave region (Figures 3d, 3e and 3f). As the estimate of the TX forced dynamic component shows very weak amplitude over northwestern North America (Text and Figure S3 in Supporting Information S1), the total forced contribution is mainly given by the sum of the RES_{FRC} and RES_{TRD} terms (~1.6°C). This estimate is within the range (1.2 – 2.8°C) suggested by Philip et al. (2021). The TX total residual component is therefore dominated by the internal variability contribution (~64% of the total residual) and shows warming in western Canada and northern part of the central U.S and localized cooling along U.S coastal areas and in New Mexico. All these results suggest that the heatwave magnitude would have been a record extreme even in a counterfactual world without human influence (14.2°C compared to the observed 15.8°C).

We now assess the uncertainty associated with the estimation of the dynamic component based on the dynamical adjustment model framework described in section 2.3.3. A preliminary step is to verify the ability of CESM2 to simulate heat extremes comparable with observed ones for western Canada and the northwest U.S states. A simple approach is to scan the 20 CESM2 historical simulations searching for TX extremes with a magnitude similar (or close) to that of observed ones when a blocking High is present over the heatwave region. Scanning through the CESM2 simulations, we find 24 3-day periods that are near analogues of the observed late June 2021 period (Text and Figure S4 in Supporting Information S1). Among these 24 simulated extreme periods, the model TX maximum is similar to the observed 2021 TX maximum with a value of ~37.1°C (7 simulated periods have TX values greater than 36°C). The observed Z500 averaged over the heatwave region lies in the middle of the range of the 24 simulated Z500 values. These results suggest that CESM2 is able to simulate TX extremes with similar magnitudes to the observed late June 2021 TX extreme when the simulated atmospheric circulation is a reasonable analogue of the observed Z500 Omega Block pattern.

We now apply dynamical adjustment to the CESM2 historical simulations as described in the first part of section 2.3.3. Figures 3g-i first show that CESM2 is able to reproduce the large-scale features of the observed TX dynamic component (the dipolar pattern). The regions with the largest warming and cooling are also very similar in observations and CESM2. Averaged over the heatwave region, the CESM2 dynamic component magnitude spans the 10.8–13.3°C range with an ensemble mean value of 11.8°C and a standard deviation of 0.7°C. The observed dynamic component magnitude (~11.3°C) is well within the CESM2 model range. Assuming a "models are statistically indistinguishable from the truth" paradigm, this suggests that our estimate of the observed dynamic component may be a slightly conservative one.

While the previous CESM2 analysis can also be considered as a way to assess the sensitivity of the dynamic component estimate to a limited sample of internal variability, we now specifically assess changes in the estimation of the dynamic component due to low-frequency ocean modes, such as the PDO and the AMO. In 2021, the PDO has experienced a negative phase during the whole year, with an average of -1.92 (https://www.ncei.noaa.gov/pub/data/cmb/ersst/v5/index/ersst.v5.pdo.dat) for the May-June-July period. Given that the phases of the PDO are associated with different impacts over Northwestern North America, the possibility of an even more extreme heatwave arises, had the PDO been in a positive phase. This can be investigated based on the above CESM2 dynamical adjustment framework by constraining the daily Z500 analogue search to CESM2 picntrl June and July months with either all days or days with a marked (absolute value of PDO or AMO index greater than 2 standard deviations) positive or negative phase. Based on the difference between dynamical adjustment results using days with a positive (or negative) PDO index and the one based on all days, we can estimate the sensitivity of the dynamic component to the PDO phase (idem for the AMO). Here we prefer using the picntrl simulation to make sure that PDO and AMO variations are purely due to internal variability. Figures 4a to 4d show the influence of the phase of low-frequency internal variability modes on the dynamic component. A positive PDO phase leads to additional large-scale warming over western Canada, with a significant warming increase over Alberta and Saskatchewan when compared with the cooling effect of a negative PDO phase (Figures 4a and 4b). The dynamic component spatial pattern associated with the PDO negative phase is reasonably close to that of the observed internal residual in British Columbia and Oregon and California coastal areas (Figures 4b and 3d). This suggests a possible contribution of the observed negative PDO phase to the internal residual pattern for these regions. The negative PDO contribution represents (28%) to the warming of the internal residual averaged over the heatwave region. This contrasts with the eastern part of the domain where the contribution of the negative PDO dynamic component has the opposite sign compared with that of the observed internal residual. This indicates that other factors such as land surface conditions may have contributed to the observed internal residual pattern.

The anomalous dynamic component patterns associated with AMO phases have weaker magnitude and more scattered patterns (Figures 4c and 4d). As the observed AMO for the 2021 May-June-July period is weakly positive (https://psl.noaa.gov/data/correlation/amon.us.data) with an amplitude less than 1 standard deviation, we suggest that its contribution to the observed internal residual is likely weak.

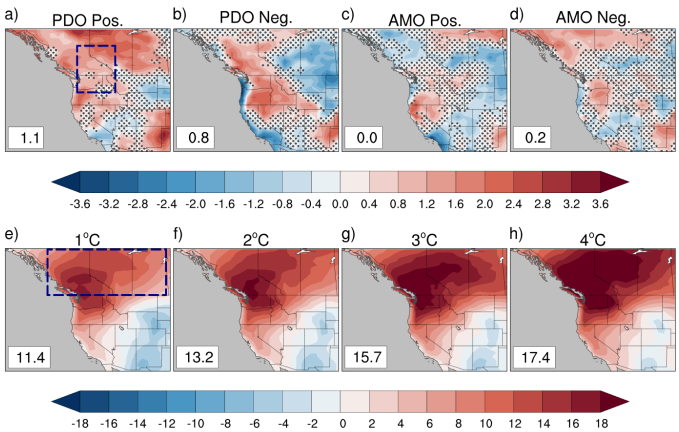

Figure 4. Mean (averaged over the 20 members) changes in the CESM2 dynamic component (TX, °C) due to the phase of low-frequency internal variability modes: (a)–(b) positive and negative phase of the PDO, (c)–(d) positive and negative phase of the AMO. (e)–(h) Total CESM2 dynamic component (TX, °C) of the heatwave at different GWLs (1, 2, 3 and 4°C) over northwestern North America. Numbers in the lower left corner indicate spatial average of the TX dynamic component: in (a)–(d) over the heatwave region (box with blue dashed line in (a)); in (e)–(h), over the extended western Canada region (box with blue dashed line in (e)). In (a)–(d), stippling indicates grid points where the CESM2 ensemble mean dynamical component is less than twice the 20–member ensemble spread. Note the different color bar scales in (a)–(d) and (e)–(h).

3.3 Heatwave dynamic component in a warmer world

Assuming that a similar atmospheric circulation anomaly to that of late June

2021 occurs in the future, we now investigate changes in the total (i.e the sum of DYN_{CF} and RES_{FRC}) dynamic component at different global warming levels (GWLs). The approach can be seen as a storyline approach with a double conditioning, one by GWL and the other one by the anomalous synoptic circulation of the June 2021 heatwave. We use different GWLs, 1, 2, 3 and 4°C. For each CESM2 historical and scenario ensemble member, we identify the timing (year) when the GWLs are reached, meaning that we search for the 20-yr time period in which change in mean global surface air temperature (GSAT) first exceeds (and remains above thereafter) a given GWL relative to the 1850–1900 climatology. The GWL-crossing year is defined as the 10th year of the 20-yr period. For each GWL period and CESM2 member, we construct an additional virtual year (in practice just the June–July period) by adding the observed June-July 2021 ERA5 Z500 anomaly to the CESM2 Z500 climatology of the GWL period. We then apply dynamical adjustment to all CESM2 members to obtain the dynamic component contributions to the (unknown) TX changes for all GWLs. Note that the model Z500 analogue search is restricted to the appropriate GWL 20-yr period and that no detrending is performed for TX and Z500. As we expect that a larger geographical domain could be strongly impacted by the heatwave at higher GWLs, we now consider a larger western Canada region for assessing the heatwave magnitude. All changes are given as differences with regard to the 1991-2020 climatology.

Figures 4e to 4h show that the magnitude of the total dynamic component averaged over western Canada strongly increases with increasing GWLs (from 11.4°C at GWL of 1°C to 17.4°C at GWL of 4°C). The region of maximum TX warming extends further eastward with increasing GWLs: with a GWL of 4°C, the area with a TX anomaly greater than 18°C (void at GWL of 1°C) covers British Columbia, Alberta and part of Saskatchewan. Western U.S States also experience additional warming with increasing GWLs, albeit to a lesser extent. The TX dipolar pattern present at 1 and 2°C GWL almost vanishes at the highest GWL. This is likely related to southward advection of warmer air masses due to the increasing Arctic amplification with increasing GWL (Figure S5a in Supporting Information S1). Sampling uncertainty linked to the use of a short 20-yr period can be estimated by looking at the dynamic component spread among the CESM2 members (Text S5 and Figure S5b in Supporting Information S1). With regard to the extended Canada region, the uncertainty of the total dynamic component pattern and magnitude (~2.4°C) does not vary much with GWL. In summary, we find that regional climate sensitivity (Senevirate and Hauser 2020) of the dynamic component scales near-linearly with GWL with a factor 2 (a 3°C increase in GWL leads to a ~6°C increase in the heatwave dynamic component).

4 Summary and Conclusions

We have performed an attribution of the late June 2021 northwestern North American heatwave based on dynamical adjustment. Our results quantify the dominant contribution of the atmospheric circulation-related component to the

spatial pattern, magnitude and persistence of the heatwave. A surface heat flux budget analysis shows the key role of atmospheric moisture and related downward clear-sky longwave flux contribution to the heatwave magnitude and persistence. This complements a previous study (Lin et al., 2022) that pointed out the role of a North Pacific atmospheric river during the week preceding the heatwave in transporting a substantial amount of moisture into the Pacific Northwest region. We find that the externally-forced contribution to the observed maximum temperature anomaly has a small magnitude (~10%) suggesting that even without human influence, the heatwave would have been a record-breaking event.

The framework proposed here provides a general template for improving physical understanding and attribution of observed extreme events without the need for any additional model simulations. However, combining dynamical adjustment with both obervations and model simulations can lead to additional insights regarding remaining issues with a purely observationally-based approach. The first added value of the joint approach is the assessment of the potential influence of unsufficient sampling of low-frequency internal variability in the estimation of the dynamic component. Based on the CESM2 large ensemble, we estimate the above uncertainty (averaged over the heatwave region) to be on the order of $\pm$ 0.7 °C (one standard deviation of the CESM2 ensemble spread). Based on a long pre-industrial control simulation, we also propose an approach to estimate the possible influence of low-frequency variability modes such as the PDO on the heatwave dynamic component. We suggest that the observed negative PDO phase in June 2021 has made a small but not negligible contribution to the heatwave spatial pattern. Finally, we show how observations and the CESM2 ensemble can be combined to suggest that regional climate sensitivity of the heatwave dynamic component, that is the response of the heatwave dynamic component to global warming level, exhibits near-linear scaling with a scale factor of two.

Acknowledgments

The author thanks the CESM2 Large Ensemble Community Project (https://www.cesm.ucar.edu/projects/community-projects/LENS2/) and supercomputing resources provided by the IBS Center for Climate Physics in South Korea.

The ERA5-related results contain modified Copernicus Climate Change Service information 2022. Neither the European Commission nor ECMWF is responsible for any use that may be made of the Copernicus information or data it contains.

Open Research

Availability Statement

The dynamical adjustment code can be found here: https://doi.org/10.5281/zenodo.5584777

All figures were made with the NCAR Command Language (NCL) version 6.6.2 (http://dx.doi.org/10.5065/D6WD3XH5).

The ERA5 data may be dowmloaded from:

Hersbach, H., Bell, B., Berrisford, P., Biavati, G., Horányi, A., Muñoz Sabater, J., Nicolas, J., Peubey, C., Radu, R., Rozum, I., Schepers, D., Simmons, A., Soci, C., Dee, D., Thépaut, J-N. (2018): ERA5 hourly data on single levels from 1959 to present. Copernicus Climate Change Service (C3S) Climate Data Store (CDS). (Accessed on < 17-02-2022 >), 10.24381/cds.adbb2d47

Hersbach, H., Bell, B., Berrisford, P., Biavati, G., Horányi, A., Muñoz Sabater, J., Nicolas, J., Peubey, C., Radu, R., Rozum, I., Schepers, D., Simmons, A., Soci, C., Dee, D., Thépaut, J-N. (2018): ERA5 hourly data on pressure levels from 1959 to present. Copernicus Climate Change Service (C3S) Climate Data Store (CDS). (Accessed on < 17-02-2022 >), 10.24381/cds.bd0915c6

Bell, B., Hersbach, H., Berrisford, P., Dahlgren, P., Horányi, A., Muñoz Sabater, J., Nicolas, J., Radu, R., Schepers, D., Simmons, A., Soci, C., Thépaut, J-N. (2020): ERA5 hourly data on single levels from 1950 to 1978 (preliminary version). Copernicus Climate Change Service (C3S) Climate Data Store (CDS). (Accessed on < 21-03-2022 >),

https://cds.climate.copernicus.eu/cdsapp#!/dataset/reanalysis-era5-single-levels-preliminary-back-extension?tab=form

Bell, B., Hersbach, H., Berrisford, P., Dahlgren, P., Horányi, A., Muñoz Sabater, J., Nicolas, J., Radu, R., Schepers, D., Simmons, A., Soci, C., Thépaut, J-N. (2020): ERA5 hourly data on pressure levels from 1950 to 1978 (preliminary version). Copernicus Climate Change Service (C3S) Climate Data Store (CDS). (Accessed on < 21-03-2022>),

https://cds.climate.copernicus.eu/cdsapp#!/dataset/reanalysis-era5-pressure-levels-preliminary-back-extension?tab=form

CESM2 model data may be downloaded from: https://www.cesm.ucar.edu/projects/community-projects/LENS2/data-sets.html.

References

Bell, B., Hersbach, H., Simmons, A., Berrisford, P., Dahlgren, P., Horányi, A., et al. (2021), The ERA5 global reanalysis: Preliminary extension to 1950. *Q. J. R. Meteorol. Soc.*, 147(741, 4186– 4227. https://doi.org/10.1002/qj.4174

Hersbach, H, Bell, B, Berrisford, P, et al., (2020), The ERA5 global reanalysis. *Q. J. R. Meteorol. Soc.*, 146: 1999– 2049. https://doi.org/10.1002/qj.3803

Lin, H., Mo, R., & Vitart, F. (2022), The 2021 western North American heatwave and its subseasonal predictions. *Geophysical Research Letters*, 49,

e2021GL097036. doi: 10.1029/2021GL097036

Lloyd, E. A. & Shepherd, T. G. (2020), Environmental catastrophes, climate change, and attribution, *Ann. N. Y. Acad. Sci.*, 1469, 105–124, https://doi.org/10.1111/nyas.14308.

Lu, J., and M. Cai (2009), Seasonality of polar surface warming amplification in climate simulations, *Geophys. Res. Lett.*, 36, L16704, doi:10.1029/2009GL040133

Neal, E., Huang, C. S. Y., & Nakamura, N. (2022), The 2021 Pacific Northwest

heat wave and associated blocking: Meteorology and the role of an upstream cyclone as a diabatic source of wave activity. Geophysical Research Letters, 49, e2021GL097699.

https://doi.org/10.1029/2021GL097699

Overland, J.E., (2021), Causes of the Record-Breaking Pacific Northwest Heatwave, Late June 2021. *Atmosphere*, 12, 1434. https:// doi.org/10.3390/atmos12111434

Philip, S. Y., Kew, S. F., van Oldenborgh, G. J., Anslow, F. S., Seneviratne, S. I., Vautard, R., et al. (2021). Rapid attribution analysis of the extraordinary heatwave on the Pacific Coast of the US and Canada June 2021. Earth System Dynamics Discussions, 2021, 1–34.

https://doi.org/10.5194/esd-2021-90

Rodgers, K. B., Lee, S.-S., Rosenbloom, N., Timmermann, A., Danabasoglu, G., Deser, C., Edwards, J., Kim, J.-E., Simpson, I. R., Stein, K., Stuecker, M. F., Yamaguchi, R., Bódai, T., Chung, E.-S., Huang, L., Kim, W. M., Lamarque, J.-F., Lombardozzi, D. L., Wieder, W. R., and Yeager, S. G., (2021), Ubiquity of human-induced changes in climate variability, *Earth Syst. Dynam.*, 12, 1393–1411, https://doi.org/10.5194/esd-12-1393-2021.

Seneviratne, S. I., & Hauser, M. (2020), Regional climate sensitivity of climate extremes in CMIP6 vs CMIP5 multi-model ensembles. Earth's Future. 8, e2019EF001474., https://doi.org/10.1029/2019EF001474

Terray, L., (2021), A dynamical adjustment perspective on extreme event attribution. *Weather Clim. Dynam.*, 2, 971–989, https://doi.org/10.5194/wcd-2-971-2021

The NCAR Command Language (Version 6.6.2) [Software]. (2019). Boulder, Colorado: UCAR/NCAR/CISL/TDD. http://dx.doi.org/10.5065/D6WD3XH5